ELSEVIER

Journal of Nuclear Materials 304 (2002) 73–82

journal of nuclear materials

www.elsevier.com/locate/jnucmat

Thermally and plastically induced residual strains in textured Zircaloy-2 plate

T.M. Holden [a], J.H. Root [a], R.A. Holt [b,*], P.A. Turner [b,1]

[a] *Steacie Institute for Molecular Sciences, National Research Council of Canada, Chalk River, ON, Canada K0J 1J0*
[b] *Atomic Energy of Canada Limited, Chalk River, ON, Canada K0J 1J0*

Received 4 April 2001; accepted 18 March 2002

Abstract

The residual intergranular strains in textured Zircaloy-2 plate samples induced by cooling from 823 K to ambient temperatures, by cold-rolling by 1.5% and 25% and by deforming in tension by 1.5% were measured by neutron diffraction. The strong rolling texture, which gives rise to two ideal orientations, permitted the interpretation of much of the data in terms of strain tensors for the two orientations. The experimental results were compared with calculations based on the elasto-plastic self-consistent model with no adjustable parameters. Close agreement was obtained for samples in the as-cooled state and deformation in tension by 1.5% but the agreement is less satisfactory for cold-rolling. © 2002 Published by Elsevier Science B.V.

1. Introduction

When polycrystalline solids are loaded beyond their yield point the anisotropy of the deformation properties of the grains with respect to crystallographic direction and the anisotropy of the single crystal elastic constants always generates stresses between the grains of different crystal orientation. These stresses are termed intergranular or type-2 stresses. Intergranular stresses are especially strong in hexagonal close-packed metals like Zircaloy-2, where the *c*-axis, [0 0 0 2], is plastically and elastically stiffer than the orthogonal $[\bar{1}\,2\,\bar{1}\,0]$ and $[1\,0\,\bar{1}\,0]$ axes. Under compression, grains whose *c*-axes are aligned with the applied stress tend to accumulate compressive stresses, whereas grains with $[\bar{1}\,2\,\bar{1}\,0\,]$ or $[1\,0\,\bar{1}\,0]$ axes aligned with the stress first deform elastically, but eventually slip and then accumulate tensile stresses to balance the stresses in the *c*-axis grains. These stresses appear experimentally after unloading as tensile and compressive residual elastic lattice strains. The presence of a prior texture also affects the behaviour since the intergranular strains will tend to be small in a direction where, for example, the grains are mostly oriented in $[\bar{1}\,2\,\bar{1}\,0]$ or $[1\,0\,\bar{1}\,0]$ directions with no constraining *c*-axis grains. In addition, in zirconium the coefficient of thermal expansion along the *c*-axis is twice as high as it is along the *a*-axis and this invariably generates thermal residual stresses.

The engineering consequences of intergranular stresses and strains coupled with strong texture may be severe. Zircaloy-2 tubing is used extensively in nuclear reactors. In the presence of a fast-neutron flux, the intergranular strains are relieved in the grains and there may be considerable macroscopic irradiation growth of the tubing since a large fraction of the grains have the same crystallographic orientation. The role of intergranular stresses in the irradiation growth of Zircaloy-2 in a fast-neutron flux was recognized by Holt and Causey [1] who developed an early model for the stresses based upon the plastic and elastic properties of the constituent grains and the texture. The model showed that, indeed, the intergranular stresses strongly modified irradiation growth.

* Corresponding author. Present address: Queen's University, Department of Mechanical Engineering, McLaughlin Hall, Stuart Street, K7L 3N6 Kingston, ON, Canada.

[1] Present address: University of Rosario, Pellegrini 250, Rosario, Argentina.

0022-3115/02/$ - see front matter © 2002 Published by Elsevier Science B.V.
PII: S0022-3115(02)00846-2

The first experiments on thermal intergranular strains in Zircaloy-2 were carried out on rod samples by MacEwen et al. [2]. Subsequently experiments were carried out on Zircaloy-2 rod samples deformed to 0.5%, 1.5%, 2.5% and 3.5% plastic deformation in tension by MacEwen et al. [3]. The Zircaloy-2 rods had a fibre texture with about two thirds of the grains having $[\bar{1}2\bar{1}0]$ axes and one third having $[10\bar{1}0]$ crystallographic axes along the rod axis. The $[0002]$ axes are confined within about $\pm 35°$ to the equatorial plane of the rod. The thermal and deformation-induced strains are low parallel to the rod axis since the elastic and plastic properties of the vast proportion of grains are similar in this orientation. However, the strains are large perpendicular to the rod axis where, for example, grains with $[10\bar{1}0]$ and $[\bar{1}2\bar{1}0]$ axes are constrained by *c*-axis grains.

A preliminary description of some of the present experimental results was given previously [4]. The lattice spacings of the samples had been accurately measured but at that time the values of the stress-free lattice parameters for our samples of Zircaloy-2 were not accurately known, so the strains were not available. An attempt was also made to interpret the data [5] in terms of the polycrystalline model [1]. Plastic deformation had to be invoked to explain the thermal residual strains, which is now known to be unrealistic, and the model did not predict the measured strains after cold-rolling. When further, somewhat arbitrary, assumptions were made in order to obtain initial strains to calculate the irradiation response, the polycrystalline model gave a reasonable representation of the transient growth resulting from the radiation-induced creep relaxation of the intergranular strains.

Recently, the strain response in Zircaloy-2 to applied stress along the rod axis was examined in situ on a neutron spectrometer [6] for three complete loading cycles up to 0.5%, 2% and 5% plastic deformation. The residual strains were in agreement with the experiments of MacEwen et al. [3] but the work showed how the strains develop under load and extended to higher plastic deformation. Tensile deformation along the rod axis corresponds to a compressive effect perpendicular to the axis and so imposes compression on the $[10\bar{1}0]$ and $[0002]$ grain orientations. The $[0002]$ grains develop larger compressive elastic strains under load than the $[10\bar{1}0]$ grains which, once slip occurs, develop tensile elastic strains to balance the compressive effects in the $[0002]$ grains. Upon unloading, the $[0002]$ grains are left in compression and the $[10\bar{1}0]$ grains remain in tension to maintain stress balance.

The elasto-plastic self-consistent model (EPSC) of Turner and Tomé [7] represents an advance over previous models and gave a satisfactory description of the experiments of MacEwen et al. [2,3] with values of the critical resolved shear stresses for prismatic and pyramidal slip of 110 and 247.5 MPa respectively. The EPSC model was also applied the interpretation of the data of Pang et al. [6] starting with the above parameters. However, with these parameters the stress required to produce a total strain of 5% was overestimated by 30% compared with the experimental stress–strain curve. In order to simulate the loading curve up to 5% the critical resolved shear stresses had to be adjusted downward to 90 and 170 MPa for the prismatic and pyramidal deformation modes respectively. For these values of the critical resolved shear stresses, the calculated intergranular strains were smaller than experiment [6] by as much as 50%. The drastic reduction of the pyramidal critical resolved shear stress in order to model similar material was considered to be unreasonable. In order to try and resolve these difficulties within the EPSC model, the effect of allowing basal slip was examined, and was found to give a better match with the flow curve than with prismatic and pyramidal slip alone. With critical resolved shear stresses of 90, 160 and 240 MPa for prismatic, basal and pyramidal slip, a reasonable distribution of activated slip systems was found exhibiting 68% prismatic, 24% basal and 8% pyramidal slip. The calculated intergranular stresses were then also in much better agreement with experiment.

The only direct observations of basal slip reported to date in zirconium alloys have been at high temperatures, either in zirconium single crystals [8] or during cyclic loading of Zircaloy-2 polycrystals [9]. There are no direct observations of basal slip at low temperatures, however the activity of basal slip has been inferred from analysis of kink bands at 77 and 253 K [10,11]. It was shown above that effects which *resemble* basal slip are needed to account for the intergranular strains in Zircaloy-2 with rod texture and several other authors have assumed basal slip in modeling deformation of zirconium alloys at low temperatures [12–15]. Whether it actually occurs at low temperatures has yet to be verified experimentally using modern techniques.

The transient of irradiation growth of Zircaloy-2 in a fast neutron flux was described by Tomé et al. [16] with the aid of the EPSC model, making use of the present strain data on Zircaloy-2 plate to guide the choice of deformation parameters. Whereas the focus of Tomé et al. [16] was the calculation of creep and growth in a reactor environment, the emphasis in the present paper is in providing a better understanding of the experimental strain data on annealed and deformed Zircaloy-2 samples through the EPSC model. The present work is partly motivated by the need to test further the basal slip hypothesis advanced in Ref. [6]. The addition of basal slip gives a better description of the experiment, though still imperfect, than was achieved in [16].

2. Experiments

2.1. Samples

The Zircaloy-2 plate received from the manufacturer had been hot-rolled at 1116 K, air annealed for 900 s at 1116 K, cooled and conditioned. Four samples were made from the as-received material and these were vacuum-annealed at 823 K for one hour and vacuum-cooled to ambient temperature. In the above condition the 'as-cooled' sample gives the thermal residual stresses generated by the unequal coefficients of thermal expansion parallel and perpendicular to the *c*-axis upon cooling from the annealing temperature. The second sample was reduced in thickness by 1.5% by cold-rolling at room temperature. The third sample was reduced in thickness by 25% by cold rolling at room temperature. The fourth sample was subjected to a 1.5% tensile deformation along the original rolling direction of the sheet. In each case a line was scribed on the plate samples to indicate the rolling direction and then eight discs were spark-machined from the plates. The discs were then assembled to form cylinders 10 mm in diameter and 20 mm high with a common crystallographic alignment. Because the samples are small, most macroscopic stresses in the plates will have been destroyed leaving only the intergranular stresses.

2.2. Texture measurements

Measurements of crystallographic texture (see Chapter 4 of Ref. [17] for a full description of the neutron technique) were made with the L3 spectrometer at the NRU reactor at Chalk River making use of 0.15 nm neutrons reflected from the (1 1 3) planes of a germanium monochromator to avoid second-order contamination. The samples were completely bathed in the neutron beam so that any remaining macroscopic effects would average to zero. Söller slit collimators of divergence 0.6° were placed in the incident and scattered beams. The samples were oriented on a kappa goniometer and the $\{10\bar{1}0\}$, $\{0002\}$, $\{10\bar{1}1\}$, $\{10\bar{1}2\}$ and $\{\bar{1}2\bar{1}0\}$ pole figures were measured in five degree increments in tilt and rotation. The $\{10\bar{1}0\}$ and $\{0002\}$ pole figures for the 'as-cooled' sample are shown in Fig. 1 and indicate high rolling texture with the $\{10\bar{1}0\}$ poles enhanced five times higher than a random distribution in the rolling direction. Fig. 1 also shows a schematic representation of the ideal orientations in the plate. The $\{0002\}$ poles are concentrated in the normal-transverse plane with a maximum about 40° from the normal direction.

The presence of strong texture permits a measurement of the intergranular strain tensor for an assembly of grains that have nearly the same orientation because there is a one-to-one correspondence between direction in the sample and crystallographic orientation. In Fig. 1, two ideal orientations of grains are identified, corresponding to the two maxima in the $\{0002\}$ pole figure with a common $[10\bar{1}0]$ direction along the plate rolling direction. These ideal orientations have an angular spread of around ±20° and are referred to subsequently as grains 1 or 2. In the $\{10\bar{1}0\}$ pole figure for example, every region of high intensity may be identified with a specific crystal orientation for either grain 1 or 2. It is straightforward to orient the samples to access particular

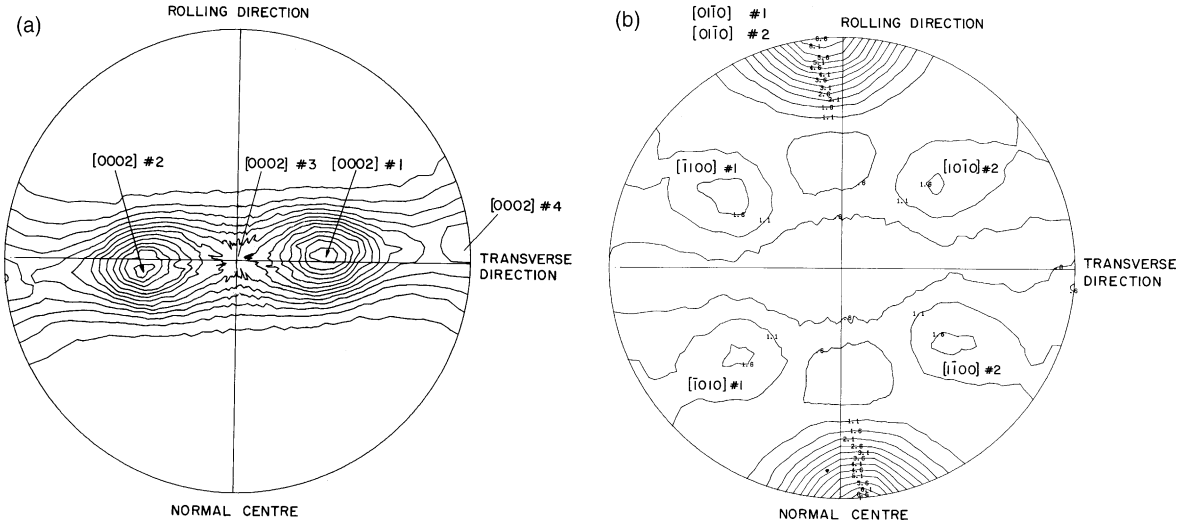

Fig. 1. A schematic representation of the principal orientations in the Zircaloy-2 plate together with the $\{10\bar{1}0\}$ and $\{0002\}$ pole figures.

reflections and hence measure the strain tensor for both grains. It is true that other grain orientations, which are not so prominent as the main ones, will also contribute at whatever angles are employed and this is fully taken into account in the EPSC model. However, the schematic diagram of Fig. 1 helps to visualize how to analyze a highly textured sample.

2.3. Strain measurements

Measurements of the residual elastic strain were made with the L3 spectrometer in a high-resolution configuration. The neutron beam, of wavelength 0.19887 nm, was reflected from the (3 3 1) planes of a germanium monochromator of mosaic 0.2° at a take-off angle of 100° with Söller collimation of 0.31° before and after the sample. Each diffraction peak was obtained by step-scanning the counter through the appropriate angular range. A calibration with three or more diffraction peaks from a standard germanium sample yielded the wavelength, λ, and the effective zero angle off-set, θ_0, of the diffractometer scale making use of Bragg's law,

$$\lambda = 2d_{\mathrm{hkil}} \sin(\theta_{\mathrm{hkil}} - \theta_0), \tag{1}$$

where the lattice spacing is denoted by d_{hkil}. The measured peak position, $2\theta_{\mathrm{hkil}}$, was obtained by fitting the observed counts versus scattering angle to a Gaussian profile on a linear background of variable slope. The precision of each peak position was between $\pm 0.003°$ and $\pm 0.017°$ depending primarily on the magnitude of the scattering angle. This lead to a precision in lattice spacing determination of, typically, ± 0.000005 nm. Measurements were made of the $\{10\bar{1}0\}$, $\{20\bar{2}0\}$, $\{0002\}$,$\{0004\}$,$\{10\bar{1}1\}$,$\{10\bar{1}2\}$ and $\{\bar{1}2\bar{1}0\}$ reflections at specific angles of tilt and orientation determined from the pole figures corresponding to grains 1 and 2. In addition to measurements on grains 1 and 2, measurements were also made for an orientation with the [0 0 0 2] axis directed along the plate normal and the $[\bar{1}2\bar{1}0]$ axis directed along the transverse direction, labeled grain 3 in Fig. 1, and for an orientation with the [0 0 0 2] axis along the transverse direction and the $[\bar{1}2\bar{1}0]$ axis directed along the plate normal, labeled grain 4 in Fig. 1. These weaker texture elements cannot be thought of as specific grains unlike the ideal orientations 1 and 2 because many different discrete crystal orientations will contribute to the average strain at any one sample orientation with no strong weighting from any one texture element. The principal crystal axes are the $[10\bar{1}0]$, $[\bar{1}2\bar{1}0]$ and [0 0 0 2] axes and the principal sample axes are the rolling direction, $\hat{r}$, the transverse direction, $\hat{t}$, and the normal direction, $\hat{n}$. Fig. 2(a) shows the angles (θ, ϕ) that define directions in the crystal axis coordinate system and Fig. 2(b) shows the angles (χ, η) that define directions in the sample axis system. Fig. 2(c) shows the relationship of the crystallographic orientations of grains 1–4 to the sample system.

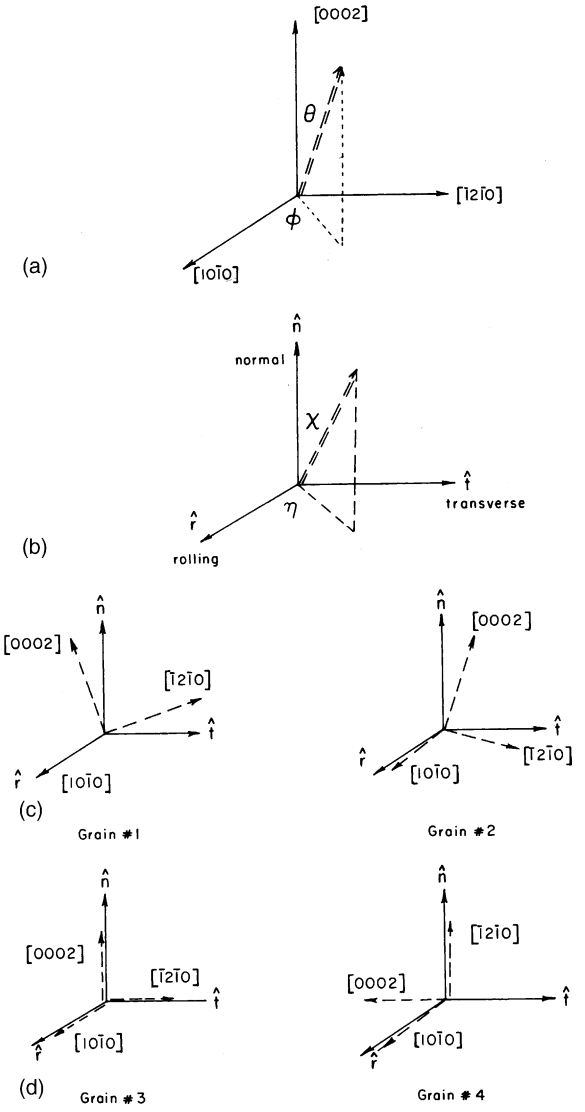

Fig. 2. (a) Angles defining directions in crystal axis coordinates. (b) Angles defining directions in sample axis coordinates. (c) Schematic representation of the four grain orientations in sample coordinates.

Accurate lattice spacing measurements require careful positioning of the sample on the centre of the goniometer which is, in turn, centred in the neutron beam. After optical alignment, to check for slight eccentric motions of the sample on the goniometer at different tilt angles, the value of the effective zero of scattering angle, θ_0, was obtained for each sample from the peak positions of twelve pairs of first and second order reflections distributed over the full range of tilts. A typical average value of θ_0 for an individual sample is $-0.003° \pm 0.005°$,

where the uncertainty is the rms spread for the twelve pairs of reflections. Systematic variations of θ_0 with tilt were absent which showed that the samples were accurately centred.

2.4. Stress-free lattice spacings

Strains, ε_{hkil}, may be determined from the measured lattice spacings, d_{hkil}, if the values of the stress-free lattice spacings, d^0_{hkil}, are known, as follows:

$$\varepsilon_{hkil} = \frac{d_{hkil} - d^0_{hkil}}{d^0_{hkil}}. \quad (2)$$

It is not possible to prepare stress-free samples of Zircaloy-2 at room temperature because of the thermal intergranular strains that develop during cooling. To determine the stress-free spacings, a coupon of the 'as-cooled' plate was measured as a function of temperature, as described in Ref. [16], taking care not to exceed the 823 K annealing temperature above which microstructure changes occur. The temperature was raised in 50 K steps and the $\{10\bar{1}0\}$ plane spacings were measured in five appropriate sample orientations at each temperature. As the temperature was raised the differences between the orientations decreased. The temperature at which the spacings all extrapolate to the same value is the stress-free temperature for which the stress-free spacing is consequently known. A similar set of measurements was also made on the $\{0002\}$ reflection. The unconstrained lattice spacings at 298 K may then be deduced from the thermal expansion of single crystal zirconium. The thermal expansion of perfect single crystals of zirconium along the *a*- and *c*-axes was also measured at Chalk River for temperatures below 850 K and found to be linear. The coefficients of expansion along the *c*- and *a*-axes are $\alpha_c = (10.3 \pm 0.2) \times 10^{-6}$ K^{-1} and $\alpha_a = (5.8 \pm 0.1) \times 10^{-6}$ K^{-1}. This procedure gave, for our sample of Zircaloy-2, stress-free values of $a_{sf}(298\text{ K}) = 0.32306$ nm and $c_{sf}(298\text{ K}) = 0.51496$ nm. These values were used to calculate strains from lattice spacings with Eq. (2).

Reference spacings for the alloy were also found by taking the derivative with respect to concentration of the interplanar spacing, $\partial(d_{hkil})/\partial C$, from polycrystalline data [18], and then calculating the changes to single crystal, i.e. unconstrained, zirconium lattice spacings generated by the chemical composition of Zircaloy-2. The values of the *a* and *c* lattice parameters of the single crystal of zirconium examined at Chalk River were 0.32340 nm [3] and 0.51479 nm [5] respectively. The two methods above for calculating reference spacings agree within an uncertainty of $\pm 1 \times 10^{-4}$ for the *a*-parameter and to within $\pm(2\text{–}3) \times 10^{-4}$ for the *c*-parameter. MacEwen et al. [2] used as reference the lattice spacings of a small crystal of Zircaloy-2 found by chance in a sample of polycrystalline material which indicated values of the *a* and *c* parameters at 300 K of 0.32306 and 0.51484 nm respectively.

3. Theory

The elasto-plastic self-consistent model was developed by Turner and Tomé [7] to predict Type-1 and Type-2 stresses and their corresponding strains. It is a numerical code based on the self-consistent scheme of Hill [19] and Hutchinson [20]. The polycrystalline aggregate is assumed to be made up of single crystals whose orientations are specified by a discrete set of Euler angles weighted to reproduce the measured crystallographic texture. The detailed plastic and elastic properties of each grain in turn are taken into account while calculating the deformation of the grain, under load or at various temperatures. Each grain is assumed to have the form of an ellipsoidal inclusion in a homogeneous medium whose properties are the average of all the other grains in the assembly. The process is iterated numerically until self-consistency is achieved. The model may be used in the plastic regime to give the overall stress and strain in the aggregate as well as those for the individual grain orientations. It may also be used to calculate the thermal strains. The model requires as input the coefficients of thermal expansion and the single crystal elastic constants, which are assumed to be identical to those of zirconium [21]. The following slip systems were considered. The primary slip system is prismatic (PR), the next most important is pyramidal (PY) and, as mentioned in the introduction, following Pang et al. [6], basal slip (BA) was also considered with critical resolved shear stresses [6] of 90 (PR), 160 (BA) and 240 (PY) MPa respectively. For a given reflection (*hkil*) and given direction in the sample (χ, η) the subset of grains in the texture that have this plane normal within 7.5° of (χ, η) was identified. For each grain in this subset, the elastic strain along (χ, η) was calculated from the grain strain tensor and the weighted average calculated. This was compared with experiment for the same diffraction peak and the same sample direction.

4. Results

The residual strains observed for grain #1 for the as-cooled, 1.5% cold-rolled, 25% cold-rolled and 1.5% tension samples are given in Figs. 3–6 as plots in crystal coordinates (θ, ϕ) for the $\{10\bar{1}0\}$, $\{0002\}$, $\{10\bar{1}1\}$,$\{10\bar{1}2\}$ and $\{\bar{1}2\bar{1}0\}$ planes. Solid symbols denote the experimental results and open symbols represent the EPSC model calculations made with the parameters adopted above, but with rolling texture calculated from the pole figures. There was no adjustment

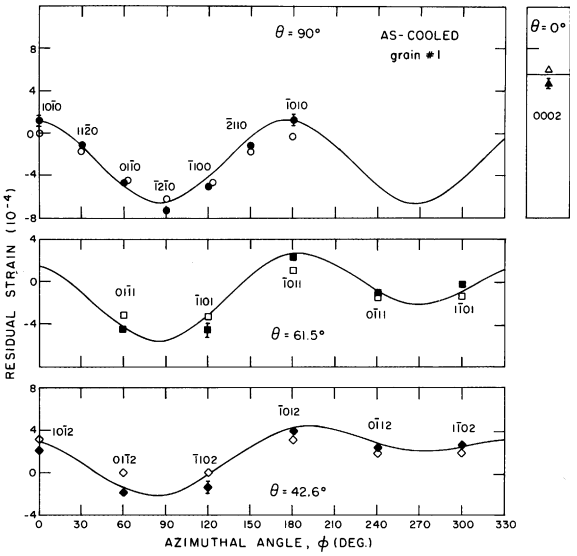

Fig. 3. Residual strains as a function of crystal angular coordinates (θ, ϕ) for grain #1 of the as-cooled Zircaloy-2 plate. Filled symbols denote experimental data, open symbols represent the EPSC calculations and the curves represent the best least-squares fit of the experimental data to a tensor form for strain. The strain data are also labeled by the corresponding (*hkil*) plane in the crystal coordinate system.

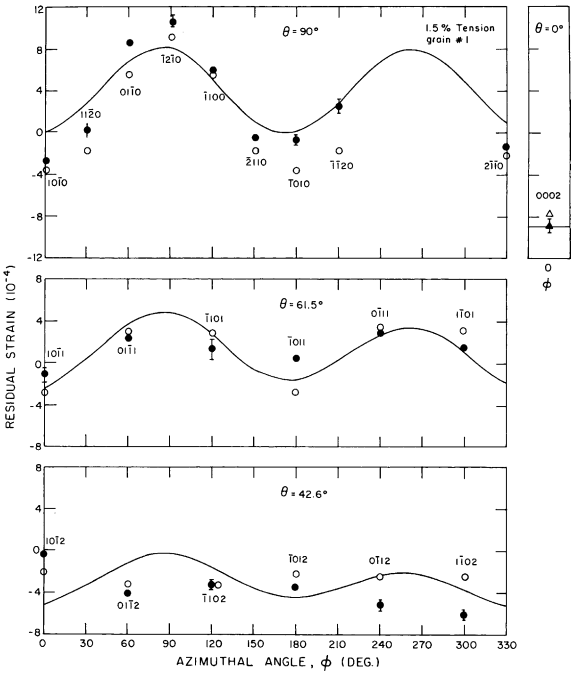

Fig. 4. Residual strains as a function of crystal angular coordinates (θ, ϕ) for grain #1 of the Zircaloy-2 plate deformed in tension by 1.5% along the rolling direction. Filled symbols denote experimental data, open symbols represent the EPSC calculations and the curves represent the best least-squares fit of the experimental data to a tensor form for strain. The strain data are also labeled by the corresponding (*hkil*) plane in the crystal coordinate system.

of parameters to describe the present experimental results. To within the experimental accuracy, the $\langle 10\bar{1}0\rangle$ and $\langle \bar{1}2\bar{1}0\rangle$ orientations give the strains in the basal plane equally well i.e. one set of reflections is not offset systematically with respect to the other in strain. The curves in the figures represent the least squares fits to the general form for a strain tensor written in crystal coordinates,

$$\varepsilon(\theta,\phi) = (\varepsilon_{11}\cos^2\phi + \varepsilon_{22}\sin^2\phi)\sin^2\theta + \varepsilon_{33}\cos^2\theta + \varepsilon_{12}\sin^2\theta\sin 2\phi + \varepsilon_{23}\sin 2\theta\sin\phi + \varepsilon_{31}\sin 2\theta\cos\phi. \quad (3)$$

The strain tensor elements for grains 1 and 2 are given in Table 1. The diagonal elements of the strain tensor for grains 1 and 2 in each case agree with each other. The ε_{11} elements along the rolling direction are small for which the rolling texture is responsible. This occurs since the very small volume fraction of grains with *c*-axes parallel to the rolling direction provides little thermal and mechanical constraint to the predominant volume fraction of $[10\bar{1}0]$ oriented grains. Perpendicular to the rolling direction there are both $\langle 0002\rangle$ and $\langle \bar{1}2\bar{1}0\rangle$ crystal axes which constrain each other and give the thermally and mechanically induced residual strains. The off-diagonal element, ε_{23}, was found to be non-zero in several cases and changed sign between grain 1 and grain 2. This result is a necessary consequence of the symmetry of the rolled plate since it is only when there is a change of sign between the two grains that the strains resolved along the plate normal direction and the transverse direction are equal. The fact that these changes of sign are observed gives confidence that the assignment of crystal orientations is correct and that the accuracy of the measurements is high. The maximum and minimum thermal strains, viz. $+4.6\times10^{-4}$ and -7.5×10^{-4}, are similar to those observed for rod texture by Pang et al. [6].

The thermal strain tensors and the deformation strain tensors are quite different since the diagonal elements ε_{22} and ε_{33} change sign. The changes in the diagonal elements for 1.5% tension, in units of 10^{-4}, are -1.1 ± 1.0, $+14.4 \pm 1.8$, -14.6 ± 1.9 which are close to the changes generated by tension in rod-textured Zircaloy-2 [2,6]. In applying tensile stress along the rolling direction we are effectively generating an elastic Poisson compression in grains which have [0002] and $[\bar{1}2\bar{1}0]$ axes perpendicular to the rolling direction: the latter eventually slip and acquire a tensile stress to balance the [0002] compression. On removal of the applied stress, the [0002] directions are left in compression and

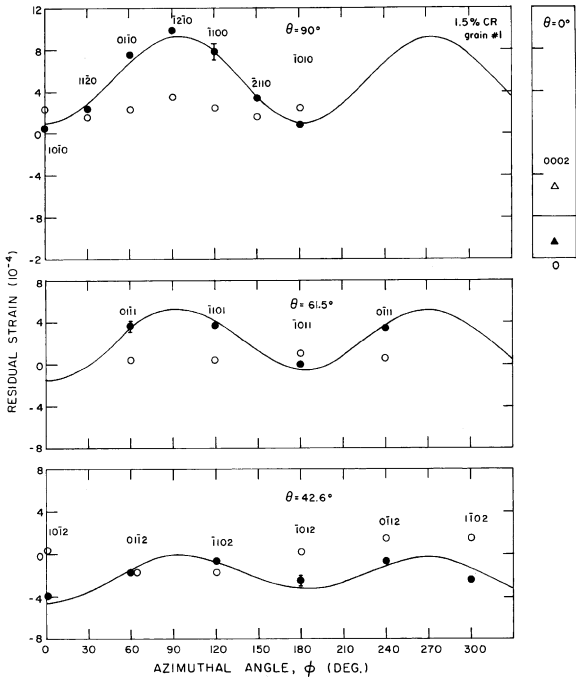

Fig. 5. Residual strains as a function of crystal angular coordinates (θ, ϕ) for grain #1 of the Zircaloy-2 plate deformed by cold-rolling by 1.5%. Filled symbols denote experimental data, open symbols represent the EPSC calculations and the curves represent the best least-squares fit of the experimental data to a tensor form for strain. The strain data are also labeled by the corresponding (*hkil*) plane in the crystal coordinate system.

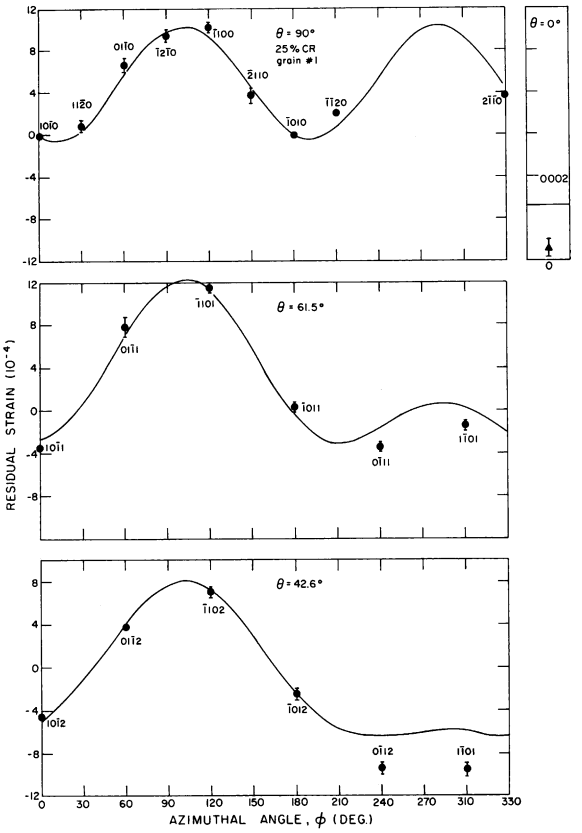

Fig. 6. Residual strains as a function of crystal angular coordinates (θ, ϕ) for grain #1 of the Zircaloy-2 plate deformed by cold-rolling by 25%. Filled symbols denote experimental data and the curves represent the best least-squares fit of the data to a tensor form for strain. The strain data are also labeled by the corresponding (*hkil*) plane in the crystal coordinate system.

there is compensating tension along the $[\bar{1}2\bar{1}0]$ directions.

Sufficient data were obtained to map the strains onto a quarter pole-figure for the $\{10\bar{1}0\}/\{\bar{1}2\bar{1}0\}$ and $\{0002\}$ reflections. Measurements made in completely different sample directions (χ, η) which were equivalent by symmetry were found to agree within the stated experimental errors and were averaged and plotted for the as-cooled, 1.5% and 25% cold-rolled samples in Fig. 7. Unfortunately, the same data were not available for the sample pulled in tension by 1.5%. The results are shown as a function of the angular deviation from the rolling direction around the periphery of the pole-figure and along a locus within the pole-figure from the rolling direction (see inset to Fig. 7) and they are also labeled by (χ, η) coordinates. The experimental results are indicated

Table 1
Strain tensors in units of (10^{-4}) for the ideal orientations in Zircaloy-2 plate

Grain description	ε_{11}	ε_{22}	ε_{33}	ε_{12}	ε_{23}	ε_{31}
As-cooled grain #1	1.1 ± 0.4	-6.6 ± 0.5	5.6 ± 0.6	-0.5 ± 0.4	-2.1 ± 0.4	-0.7 ± 0.5
As-cooled grain #2	1.4 ± 0.6	-7.4 ± 0.5	5.8 ± 0.6	-0.6 ± 0.3	2.5 ± 0.4	-0.4 ± 0.4
1.5% T grain #1	0.0 ± 1.0	7.8 ± 1.3	-9.0 ± 1.3	1.1 ± 0.9	1.0 ± 1.0	-0.4 ± 1.0
1.5% T grain #2	0.9 ± 1.6	7.5 ± 1.5	-9.4 ± 1.5	0.5 ± 1.0	-1.1 ± 1.0	0.0 ± 1.1
1.5% CR grain #1	1.1 ± 0.5	9.2 ± 0.5	-8.1 ± 0.6	-0.4 ± 0.3	0.1 ± 0.3	-0.6 ± 0.4
1.5% CR grain #2	1.7 ± 0.5	9.8 ± 0.3	-9.0 ± 0.5	0.5 ± 0.2	-0.4 ± 0.3	-0.5 ± 0.3
25.0% CR grain #1	0.0 ± 0.8	9.9 ± 1.2	-6.8 ± 1.4	-2.3 ± 0.8	6.9 ± 0.8	-1.4 ± 0.8
25.0% CR grain #2	0.3 ± 0.7	11.1 ± 0.5	-11.4 ± 0.5	-0.4 ± 0.3	-9.5 ± 0.4	-0.9 ± 0.4

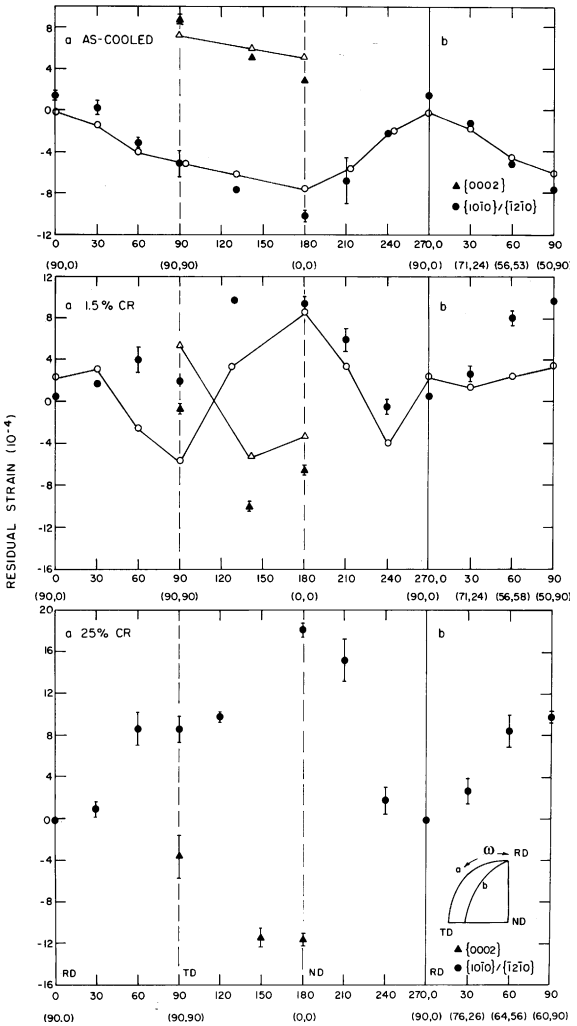

Fig. 7. Angular variation of the residual strain in pole-figure coordinates (χ, η) plotted as a function of angular deviation from the rolling direction for a locus (a) around the edge of the pole-figure and for a locus, (b) within the pole-figure (see inset) for the as-cooled, 1.5% cold-rolled and 25% cold-rolled samples. Experimental results are designated by filled circles for the $\{1\,0\,\bar{1}\,0\}$ or $\{\bar{1}\,2\,\bar{1}\,0\}$ reflections and filled triangles for $\{0\,0\,0\,2\}$ reflections. The corresponding EPSC results are designated by open circles and triangles joined by lines.

by solid symbols and the EPSC calculations by open symbols joined by lines. The agreement between the experiment and the model with no adjustable parameters is very close for the as-cooled sample but not so good for the 1.5% cold-rolled sample. In this case, the model gives the correct trends for the strains starting from the as-cooled condition but does not go far enough as was the case for the ideal orientations shown in Fig. 5. The results for the 25% cold-rolled sample show the same trends as the 1.5% cold-rolled sample, but the amplitude of the strain variation is larger. Because of the very large plastic deformation the EPSC model is not valid in this case.

5. Discussion

There is close agreement, as shown in Fig. 3, between the experiment and the EPSC model for the as-cooled sample for grain #1. The agreement is equally good for grain #2, although the data are not shown. Plasticity is not required for the thermal strains since elastic processes among the grains can account entirely for the results as found previously in the analysis of Turner and Tomé [7]. This is the result of using the self-consistent model instead of an upper-bound model [1,5]. The curve in Fig. 3 represents the fit to a tensor form for the strain in the axis system defined by $[1\,0\,\bar{1}\,0]$, $[\bar{1}\,2\,\bar{1}\,0]$ and $[0\,0\,0\,2]$ and it provides a good description of the data. The question arises: to what extent does this accurately represent the strain tensor for the grain since there will be other grain orientations contributing to the strain? The EPSC model results were fitted to the tensor form, Eq. (3), and the elements were found to be in good agreement with the experimental values.

Fig. 8 shows the experimental strain tensors for grains 1 and 2 plotted in a pole figure representation for the as-cooled sample. Note that the tensile $[\bar{1}\,2\,\bar{1}\,0]$ strain for grain #2 occurs in nearly the same direction as the compressive $[0\,0\,0\,2]$ strain for grain #1. Since zirconium is fairly isotropic elastically, this implies that stress-balance is achieved by the balance of grain #1 against grain #2. It is interesting to note that the strains directed along the sample principal axes ($\hat{r}$, $\hat{t}$, $\hat{n}$) are not very large. If the strains had only been measured along the sample principal axes, the large intergranular strains would have been missed. The principal intergranular residual strains tend to be close to the principal crystal axes which was also the case for rod-textured Zircaloy-2 [2,3,6].

One feature predicted by the model is that the maximum $[0\,0\,0\,2]$ residual strain associated with cooling (Fig. 7) is not observed along the maximum in the texture distribution, i.e. at 40° to the sample normal, but is observed along the transverse direction in the plate, where the strain is about 30% larger. The minimum $[0\,0\,0\,2]$ strain, 40% smaller than the value at the peak of the texture, is observed in the normal direction, and this is also predicted by the model. Three factors affect the value of the strain, the volume fraction of $[0\,0\,0\,2]$ grain orientations, the volume fraction of grains constraining the $[0\,0\,0\,2]$ grains (principally those associated with the ideal grain orientations) and the crystallographic direction of these grains (since this determines both the coefficient of expansion and the elastic properties). For example, the $[\bar{1}\,2\,\bar{1}\,4]$ crystal directions are strongly rep-

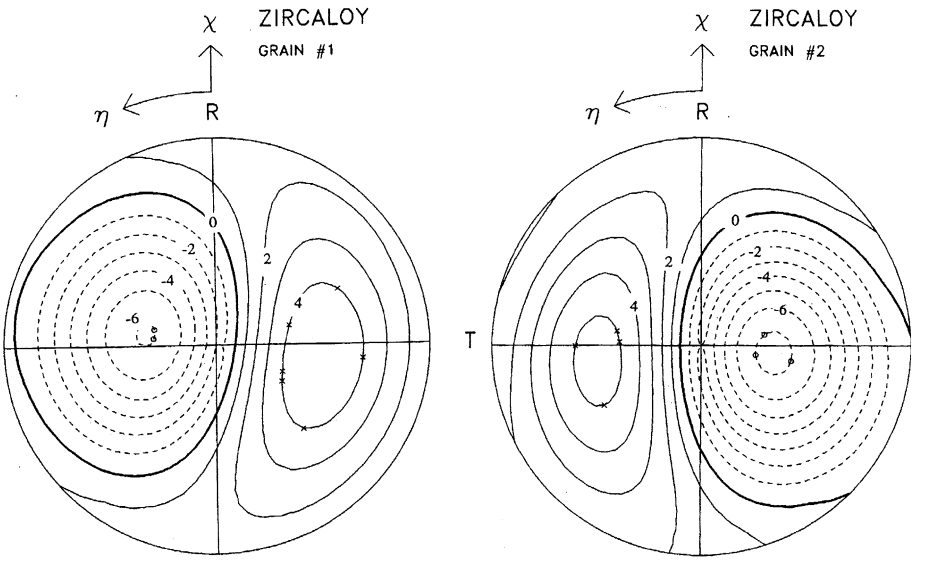

Fig. 8. Strain tensors derived from the fits to the strain data for grains 1 and 2 of the as-cooled sample plotted in a pole-figure representation.

resented along the plate normal and these have a coefficient of expansion which is only 17% less than that for the [0 0 0 2] grains, thus giving rise to a relatively small thermal strain. This compares with a coefficient of expansion that is 27% less than that for [0 0 0 2] grains along the transverse direction in the sheet.

The results in Figs. 4 and 7, for the sample deformed 1.5% in tension, show that the EPSC model agrees very well with experiment with no adjustable parameters. The root mean square deviation of experiment from the model calculation for the 1.5% tension sample with the critical resolved stress parameters of Pang et al. [6] is 1.7×10^{-4} whereas the values for the sets optimized for the 1.5% tension and 1.5% cold-rolled samples by Tomé et al. [7] are both 3.0×10^{-4}. The root mean square deviation of theory from experiment for the 1.5% cold-rolled sample with the parameters of Pang et al. [6] is much worse, (5×10^{-4}), than for the 1.5% tension sample but is much better than the deviations from the sets of parameters optimized [7] for the 1.5% tension and 1.5% cold-rolled samples, which are 9×10^{-4} and 7×10^{-4} respectively. The critical resolved shear stresses suggested by Pang et al. [6] including basal slip therefore appear to be superior to those suggested earlier by Tomé et al. [7]. The arrangement of plastically hard and soft grains perpendicular to the stress axis is quite similar to the case of rod textured Zircaloy-2 and the physical explanation of the strains is similar to that case. The result shows that once the modes of deformation are identified the results are independent of the details of the texture. The EPSC model calculation gives a good estimate of the behaviour of all the grains not just those associated with the ideal orientations.

The model calculation for the plate deformed by rolling to 1.5% shown in Figs. 5 and 7 is not in good agreement with experiment. The model deviations away from the thermal stress state have the same signs as the experiment but are too small by between 30% and 50%. As in the previous cases, the strain in the rolling direction remains small relative to the strains in the perpendicular directions.

Compression along the normal direction should lead to compressive strains in [0 0 0 2] grains oriented in this direction, since these are constrained primarily by the [$\bar{1}$ 2 $\bar{1}$ 4] grain orientations of the ideal orientation which are plastically and elastically softer than [0 0 0 2] grains and would be expected to go into tension. Theory and experiment are in agreement in this case. Compression along the normal direction corresponds to a tensile effect on [0 0 0 2] grains lying perpendicular to this direction, in particular along the transverse direction. This might be expected to lead to tensile residual strains in [0 0 0 2] grains in the transverse direction and this is what the EPSC model predicts. Experiment, however, indicates that the transverse [0 0 0 2] strains are close to zero for the 1.5% cold-rolled sample and compressive for the 25% cold-rolled sample. However, twinning was not included in the model calculation and is likely to provide an alternative mode of *c*-axis deformation to simple elastic strain. It was shown [22] that much smaller residual strains are generated by compressive plastic deformation than by tensile plastic deformation in rod-textured Zircaloy-2 and twinning was invoked to explain

this and the texture changes generated by deformation in compression. Twinning was subsequently observed under this condition [23]. One might expect that the $[10\bar{1}0]$ strain in the rolling direction to be small since there is no constraint in this direction.

A model calculation for 25% reduction by rolling is outside the validity of the EPSC model which assumes that the elastic and plastic deformations are roughly comparable. In this case a viscoplastic approach [24] is required. Only the experimental results for 25% cold-rolling are presented in Figs. 6 and 7 together with the fits to a strain tensor in crystal coordinates. Comparing the magnitude of the elements of the strain tensor for the 1.5% and 25% cold-rolled samples shows that the magnitudes of the diagonal elements do not change markedly with deformation but the ε_{23} shear term increases very strongly. The feature of the experimental data for grain #1 that corresponds to this increase is the tensile shift of the $\{10\bar{1}1\}$ and $\{10\bar{1}2\}$ strains between $\phi = 0°$ and 180° and a corresponding compressive shift between 180° and 360°.

6. Conclusions

1. Residual strains are observed in plate-textured Zircaloy-2 which are very similar in magnitude to those previously reported for rod texture.
2. Because of the strong texture it is possible to determine the intergranular strain tensors from the data for the two ideal orientations.
3. There is excellent agreement with the EPSC model with no adjustable parameters for the as-cooled and 1.5% tension samples. This supports the hypothesis of a mode of deformation resembling basal slip.
4. There is poor agreement with the 1.5% cold-rolled sample. It is suggested that twinning as a mode of deformation should be included for compressive deformation.
5. For the 25% cold-rolled sample the diagonal elements of the strain tensor are similar in magnitude to the results for much smaller amounts of cold work, but the off-diagonal terms are much larger.

Acknowledgements

We wish to acknowledge the expert technical assistance of M.M. Potter, D.C. Tennant, A.H. Hewitt and H.F. Nieman. The late V. Fidleris was instrumental in initiating the study of intergranular strains with neutron diffraction as a way of eventually understanding the creep and growth of zirconium alloys. We wish to thank C.N. Tomé for many useful discussions about these experiments.

References

[1] R.A. Holt, A.R. Causey, J. Nucl. Mater. 150 (1987) 306.
[2] S.R. MacEwen, C.N. Tomé, J. Faber Jr., Acta Metall. 37 (1989) 979.
[3] S.R. MacEwen, N. Christodoulou, A. Salinas-Rodriguez, Metall. Trans. A 21A (1990) 1083.
[4] T.M. Holden, J.H. Root, V. Fidleris, R.A. Holt, G. Roy, Mater. Sci. Forum 27&28 (1988) 359.
[5] R.A. Holt, T.M. Holden, A.R. Causey, V. Fidleris, in: J.B. Bilde-Sorensen, N. Hansen, D. Juul-Jensen, T. Leffers, H. Lilholt, O.B. Pedersen (Eds.), Proceedings of the 10th Risø International Symposium on Metallurgy and Materials Science, Risø National Laboratory, Roskilde, Denmark, 1989, p. 383.
[6] J.W.L. Pang, T.M. Holden, P.A. Turner, T.E. Mason, Acta Mater. 47 (1999) 373.
[7] P.A. Turner, C.N. Tomé, Acta Metall. Mater. 42 (1994) 4143.
[8] A. Akhtar, Acta Metall. 21 (1973) 1.
[9] L. Xiao, H. Gu, Scr. Metall. Mater. 30 (1994) 175.
[10] J.L. Martin, R.E. Reed-Hill, Trans. Metall. Soc. AIME 230 (1964) 780.
[11] R.E. Reed-Hill, in: R.E. Reed-Hill, J.P. Hirth, H.C. Rogers (Eds.), Deformation Twinning, vol. 25, Gordon and Breach, New York, 1964, p. 295.
[12] A. Salinas Rodriguez, Acta Metall. Mater. 43 (1995) 465.
[13] R.A. Lebensohn, P.A. Turner, J.W. Signorelli, C.N. Tomé, in: T. Ericsson, M. Odén, A. Andersson (Eds.), Proceedings of Fifth International Conference on Residual Stresses (ICRS-5), Linköping University, Linköping, 1997, p. 460.
[14] R.E. Loge, J.W. Signorelli, Y.B. Chastel, M.Y. Perrin, R.A. Lebensohn, Acta Mater. 48 (2000) 3917.
[15] N. Christodoulou, E.T.C. Ho, C.K. Chow, M. Resta-Levi, Metall. Mater. Trans. A 31 (2000) 409.
[16] C.N. Tomé, N. Christodoulou, P.A. Turner, M.A. Miller, C.H. Woo, J.H. Root, T.M. Holden, J. Nucl. Mater. 227 (1996) 237.
[17] U.F. Kocks, C.N. Tomé, H.-R. Wenk, Texture and Anisotropy, Cambridge University, Cambridge, 1998.
[18] D.L. Douglass, The Metallurgy of Zirconium, Atomic Energy Review Supplement 1971, International Atomic Energy Agency, Vienna, 1971 p. 3.
[19] R. Hill, J. Mech. Phys. Solids 13 (1965) 89.
[20] J.W. Hutchinson, Proc. Roy. Soc. Lond A 319 (1970) 247.
[21] E.S. Fisher, C.J. Renken, J. Nucl. Mater. 4 (1988) 311.
[22] S.R. MacEwen, N. Christodoulou, C.N. Tomé, J. Jackman, T.M. Holden, J. Faber Jr., R.L. Hitterman, in: J.S. Kallend, G. Gottstein (Eds.), Proceedings of 8th International Conference on Textures of Materials, The Metallurgical Society, Warrendale, PA, 1988, p. 825.
[23] V. Perovic, G.C. Weatherly, S.R. MacEwen, M. Leger, Acta Metall. Mater. 40 (1992) 363.
[24] R.A. Lebensohn, P.V. Sanchez, A.A. Pochettino, Scr. Metall. Mater. 30 (1994) 481.